Published in final edited form as:
J Am Chem Soc. 2009 October 28; 131(42): 15257–15261. doi:10.1021/ja9047043.

Design, synthesis, and testing of difluoroboron derivatized curcumins as near infrared probes for *in vivo* detection of amyloid-β deposits

Chongzhao Ran[1], **Xiaoyin Xu**[2], **Scott B. Raymond**[3], **Brian J. Ferrara**[3], **Krista Neal**[3], **Brian J. Bacskai**[3], **Zdravka Medarova**[1], and **Anna Moore**[*,1]

[1]Molecular Imaging Laboratory, MGH/MIT/HMS Athinoula A. Martinos Center for Biomedical Imaging, Department of Radiology, Massachusetts General Hospital/Harvard Medical School, Room 2301, Building 149, Charlestown, Boston, Massachusetts 02129

[2]Optical Imaging Laboratory, Department of Radiology, Brigham and Women's Hospital, Boston, MA 02115

[3]Alzheimer's Disease Research Unit, Department of Neurology, Massachusetts General Hospital

Abstract

Amyloid-β (Aβ) deposits have been identified as key players in the progression of Alzheimer's disease (AD). Recent evidence indicates that the deposits probably precede and induce the neuronal atrophy. Therefore, methods that enable monitoring the pathology before clinical symptoms are observed would be beneficial for the early AD detection. Here, we report the design, synthesis, and testing of a curcumin derivatized near infrared (NIR) probe CRANAD-2. Upon interacting with Aβ aggregates, CRANAD-2 undergoes a range of changes, which include a 70-fold fluorescence intensity increase, a 90 nm blue-shift (from 805 nm to 715 nm), and a large increase in quantum yield. Moreover, this probe also shows a high affinity for Aβ aggregates (Kd = 38.0 nM), a reasonable Log P value (Log P = 3), considerable stability in serum and a weak interaction with albumin. After intravenous injection of this probe, 19-month old Tg2576 mice exhibited significantly higher relative signal than that of the control mice over the same period of time. In summary, CRANAD-2 meets all the requirements for a NIR contrast agent for the detection of Aβ plaques both *in vitro* and *in vivo*. Our data point towards the feasibility of monitoring the progress of the disease by NIR imaging with CRANAD-2. In addition, we believe that our probe could be potentially used as a tool for drug screening.

Introduction

Amyloid-β (Aβ) deposits are a pathological hallmark of Alzheimer's disease (AD). Their formation arises from the aggregation of peptides Aβ40 and Aβ42, which are generated from amyloid peptide precursor (APP) by cleavage with β- and γ-secretases.[1] Although the assertion that Aβ deposits precede and induce neuronal atrophy remains controversial,[2] recent evidence indicates that Aβ plaques are a critical mediator of neuritic pathology.[3] Currently, memory and behavioral tests are widely used for late-stage AD diagnosis;[4] however, early detection at the asymptomatic syndrome stage still presents a challenge. Molecular imaging, a detection

amoore@helix.mgh.harvard.edu.

Supplemental information available: general material and methods, Log P measurement, stability test in serum, BSA interaction, histological evaluation, full lists of reference ([4]) and ([5]), and supplemental figures. This material is available free of charge via the Internet at http://pubs.acs.org.

technique with sensitivity at the molecular level, represents a promising approach to face this challenge. Magnetic resonance imaging (MRI), positron emission tomography (PET), and optical imaging have each been employed for the early detection of AD pathology, and considerable progress has been achieved in recent years.[5–13] Although studies indicate that molecular MRI is a promising diagnostic modality, its low sensitivity could be an obstacle for its application in the clinic. In recent years, it has been demonstrated that PET can also be used as a powerful imaging modality to detect AD pathology; however, its high cost and the narrow isotope availability of PET probes limit its broad usage. [5] Molecular optical imaging, including multiphoton and near infrared imaging, has been used to detect early AD pathology in animal models. The invasiveness and small field-of-view of multiphoton imaging limit its application, and this approach is not translatable for clinical imaging. [5,8,14–16] Near infrared imaging (NIR) is an attractive tool for early AD detection because of its acceptable depth penetration, non-invasive operation, and inexpensive instrumentation. Though NIR imaging is so far limited to animal studies, some NIR probes could be easily modified to PET imaging probes, and thus are worth pursuing. In addition, new optical imaging systems such as fluorescent molecular tomographic (FMT) imaging are being developed for clinical applications. [17] While several non-NIR molecules that specifically bind to senile plaques have been reported for multiphoton imaging and histological studies, [5,14,18] only few near-infrared probes have been reported thus far.[6,8,19]

In principle, a good NIR probe for senile plaques should have the following properties:[5,8] 1) specificity to Aβ plaques; 2) reasonable lipophilicity (Log P is between 1–3); 3) molecular weight less than 600 dalton; 4) emission wavelength >650 nm and a large Stokes shift; 5) high affinity binding; 6) high quantum yield; 7) low affinity binding with BSA; 8) reasonable stability in blood; 9) straight-forward synthesis; and most importantly, 10) upon binding to Aβ plaques, it should significantly change its fluorescence properties (i.e., fluorescence intensity, fluorescence lifetime, emission wavelength and quantum yield). An increase in fluorescence intensity means that the probe will be “turned on” upon interacting with a target. To date, none of the reported NIR probes meet all of these criteria. Although the oxazine-derivative probe AOI 987 was reported as an efficient NIR probe for detecting and monitoring senile plaques, it has a small Stokes shift (25 nm) and moderate binding (Kd = 220 nM).[6] Moreover, it displayed a slight fluorescence intensity decrease instead of significant fluorescence intensity increase upon binding with Aβ aggregates. NIAD-4 was reported as a senile plaque-specific probe for two-photon microscopy, and could be used as a NIR probe as well. [8] Additionally, Li et al. reported that some styryl dyes could be “turned on” upon incubation with Aβ aggregates, but these compounds may have little chance of penetrating the blood brain barrier (BBB) because of their high polarity.[18]

Curcumin, a brightly colored powder, is the principal curcuminoid of the Indian curry, and has been consumed daily for thousands of years in India and other regions. Curcumin is known for its antitumor, antioxidant, antiarthritic and anti-inflammatory properties. [20–23] It has been utilized as an anti-amyloid agent as well. [14,24] In 2004, Yang et al. reported that curcumin could be used as a histological staining reagent for senile plaques and showed that curcumin could decrease amyloid deposits *in vivo*. [24] Further, Garcia-Alloza et al. demonstrated by two-photon imaging that curcumin could be visualized *in vivo* and could prevent the progress of amyloid plaque formation in APP-tau transgenic mouse model. [14] In addition, Ryu suggested that curcumin derivatives were potential PET probes for amyloid imaging. [25] All of the studies demonstrate that curcumin has some specificity for amyloid plaques and displays high-affinity binding for Aβ aggregates (Kd = 0.20 nM). [25] However, curcumin is not a practical probe for *in vivo* NIR imaging because of its short emission wavelength, limited access across blood-brain barrier, and rapid metabolism. [25] Despite these limitations, we hypothesized that, by modifying the structure of curcumin, it would be possible to shift the emission wavelength to the NIR range and create a probe with significant changes in fluorescence properties upon

binding to plaques that had a better PK profile and was less susceptible to metabolic degradation. Here we report on the design, synthesis, and testing of curcumin derivatives as NIR imaging probes that meet all of the above-mentioned criteria.

Results and discussions

Design, synthesis and spectra of probes

The rationale behind the design of our NIR probe was based on three facts. First, it is a known phenomenon that curcumin reacts with boric acid to form a red colored compound rosocyanine, which consists of two curcumins connected by a borate ring. [26,27] The color change from yellow (curcumin) to red (rosocyanine) indicates an absorption red shift, which may be ascribed to the introduction of a boron atom ($\pi \rightarrow \pi^*$ from oxygen to empty orbital of boron) into the rosocyanine molecule. We hypothesized that we could utilize the red shift benefit of boron incorporation to design boron-containing curcumin derivatives with emission in the 650–900 nm range. Second, although 2,2-difluoro-1,3,2-dioxaborines are known compounds and their fluorescence properties have been characterized,[28–32] the fluorescence change caused by difluoro-boronate incorporation into diketone remains unclear. Nonetheless, introduction of difluoro-boronate ring into dipyrromethene systems form well-documented red-shifted Bodipy dyes.[33] Therefore, it was reasonable to speculate that, by incorporating a difluoro-boronate moiety into curcumin, it would generate an appropriate red shift. Finally, *N,N'*-dimethyl group is well-known as the best absorption red-shift pushing group for *para*-substituted aromatic ring. [34] We accordingly further proposed to modify curcumin by replacing the phenolic hydroxyl groups with *N,N'*-dimethyl groups to enable red-shifted absorption, and consequently, lead to an additional red-shift in emission (Fig. 1). Based on these considerations, probe **1** and probe **2** were designed and synthesized. Compound **1** has been reported as an HIV-1 and HIV-2 protease inhibitor, [35] and this probe was synthesized by following the reported procedure. [35,36] Compound **2** was prepared by condensation of 4-*N,N'*-dimethylbenzaldehyde with 2,2-difluoro-1,3-dioxaboryl-pentadione in acetonitrile.[29] For convenience, in the proceedings of this report, we named compound **1** as CRANAD-1, and compound **2** as CRANAD-2 (which stands for the initial and the last name of the first author (C. Ran) as well as for Alzheimer's Disease – AD).

As anticipated, there was an approximately 80 nm red shift of emission after installation of the difluoro-boron ring into the curcumin molecule (CRANAD-1). In methanol, the maximum emission of CRANAD-1 was 640 nm, while the λmax(em) of curcumin was 560 nm (SI Fig. 1A). There was also a 100 nm Stokes shift for CRANAD-1 (λmax(ex)= 540 nm, λmax(em) =640 nm), which was larger than that of curcumin's 50 nm shift (λmax(ex)= 510 nm, λmax (em) =560 nm) (data not shown). Although we achieved considerable red shift and Stokes shift with CRANAD-1, our ultimate goal was to push the emission further into NIR range. In order to do this we further modified CRANAD-1 by replacing the phenolic hydroxyl group with *N,N'*-dimethyl group to yield compound CRANAD-2.

With this replacement, the emission of CRANAD-2 was red-shifted to λmax(em) = 760 nm in methanol, which falls in the best range for NIR probes. The compound also displayed a large Stokes shift (λmax(ex)= 640 nm, λmax(em) = 805 nm) (SI Fig. 1B) in PBS. Furthermore, by comparing the fluorescence intensity in methanol, the quantum yield of CRANAD-2 was significantly higher than that of curcumin (SI Fig. 1A). As expected, the emission wavelength of CRANAD-2 displayed a typical solvent-dependency (SI Fig.1C), i.e., it showed longer emission and lower quantum yield in polar solvent. Taken together, we demonstrated that by two-step red-shift modification of curcumin, we were able to push its emission wavelength into an ideal emission range for NIR probes. Additionally, these modifications produced a large Stokes shift of CRANAD-2.

In vitro test with CRANAD-2

We tested the binding affinity and fluorescence intensities of CRANAD-2 with synthetic Aβ (1–40) aggregates in PBS (pH 7.4). While we observed weak fluorescence intensity for the probe alone in PBS, there was a remarkable 70-fold fluorescence intensity increase in the presence of Aβ40 aggregates (Fig. 2A). This result suggested that our probe could be "turned on" upon interacting with its substrate. This was further reflected by the changes in quantum yield from 0.006 in PBS to 0.40 after binding to Aβ40 aggregates. A significant blue-shift (from 805 nm to 715 nm, total shift of 90 nm, inset in Fig. 2A) was observed as well after binding with Aβ40 aggregates, possibly indicating the insertion of the dye into the hydrophobic environment of the aggregates. Taken together, CRANAD-2, upon binding to Aβ40 aggregates, displayed a "turn on" phenomenon, a quantum yield increase, and a considerable emission blue-shift.

Next, the apparent binding constant (Kd = 38.69±2.77 nM, R_2=0.9952, SI Fig. 3) of CRANAD-2 to Aβ aggregates was measured by fluorescence intensity (F.I.) with various concentrations of the probe. This binding constant was significantly higher than that of Thioflavin T, a widely used agent for detecting protein and peptide aggregation such as Aβ aggregation (Kd = 580 nM), [37] and than that of AOI 987 (Kd = 220±130 nM) 6 and was close to that of NIAD-4 (Kd = 10.0 nM), 8 and was lower than that of PiB (Kd = 4.7 nM), a PET probe under international clinic trials for Aβ deposits imaging. [5] We found no significant change in fluorescence during incubation with BSA (SI Fig. 4), suggesting that there is little or no interaction between the probe and BSA. Furthermore, we also found that the probe was stable when CRANAD-2 was incubated in human serum for 2 hours at 37°C. Both fluorescence and HPLC spectra showed about 70 % recovery of the probe, indicating its relative stability (SI Fig. 5 A–D). Additionally, we confirmed the capability of CRANAD-2 to detect Aβ plaques *in vitro* by staining brain sections from a 12-month old APP-PS1 transgenic mouse. We observed high contrast staining of plaques in the tissue, which co-localized with the signal from standard Thioflavin T stained sections (Fig. 2B–D). These results indicate CRANAD-2's specificity for Aβ plaques.

Brain blood barrier penetrating test of CRANAD-2

In order for the probe to cross blood-brain barrier, its lipophilicity (log P) should be within the 1–3 range. Our testing of the lipophilicity of CRANAD-2 resulted in a log P = 3.0, indicating that CRANAD-2 holds promise as a BBB penetrating probe. To further demonstrate the probe's BBB penetrating ability, we intravenously injected wild type mice with CRANAD-2, and measured the concentration of the dye in plasma and brain at a range of time points post-mortem. PiB, a well-studied plaque-specific PET probe, was used as a positive control,[5] while ICG, a known non-BBB penetrating probe, was used as a negative control probe. As shown in SI Fig. 6, both the fluorescence spectrum and HPLC analysis of the brain homogenate confirmed the presence of CRANAD-2 in the brain (S.I. Fig. 6B–D). CRANAD-2 displayed a rapid clearance from blood while the clearance from the brain was significantly slower. Compared to PiB, CRANAD-2 showed less entry into brain, and slower clearance. There was no detectable ICG in brain homogenates after iv injection at all time points (SI Fig. 6A).

In vivo imaging and ex vivo histology

To validate the feasibility of CRANAD-2 as a NIR imaging probe, transgenic 19-month-old Tg2576 mice were used, and aged-matched wild type littermates served as controls. Tg2576 transgenic mouse model, also known as APPswe mouse model, carries a transgene coding for the 695-amino acid isoform of human Alzheimer β-amyloid (Aβ) precursor protein (APP), and expresses high concentrations of the mutant Aβ. It develops significant amyloid plaques and displays memory deficits around 10–12 months of age. [38] Tg2576 mice have been widely used in the AD research community. In this study, we used fluorescence intensity-based NIR

imaging technique to capture mice images. For this technology, fluorescence reflectance (also known as epifluorescence) and tomography (FMT) are the two most used modalities for *in vivo* small animal imaging. Reflectance imaging is suitable for fast imaging, but has less penetrating depth (< 1 cm) and poor resolution. Although FMT has better resolution and deeper penetrating ability (< 10 cm), [17] it is still in development stage. Therefore, we chose the reflectance imaging technique to conduct the *in vivo* imaging. Mice images were recorded before and after i.v. injection of CRANAD-2 at 5.0 mg/Kg dosage. For mice with comparable background fluorescence (F_{pre}) (Fig.3A *vs* B), the fluorescence signal diminished considerably more slowly for 19-month-old Tg2576 mice than that of the control group. The fluorescence intensities of the transgenic group were higher than those of the control group at 30, 60, 120, and 240 minutes. These results were correlated to semi-quantitative analysis of the images, which was performed by selecting a region of interest (ROI) in the brain and normalizing fluorescence intensity at any given time point ($F_{(t)}$) to background fluorescence intensity before the injection ($F_{(pre)}$). For Tg2576 and control mice, the differences of normalized signal were 55%, 68%, 61%, and 70% at 30, 60, 120 and 240 minutes, respectively. Notably, our data showed that the differences between transgenic and control groups could be observed at the earliest time-point (30 min.). Finally, we confirmed the presence of CRANAD-2 by ex vivo histology. Mice were intravenously injected with 5.0 mg/kg of CRANAD-2 probe, perfused and sacrificed 2 hours after injection. We observed senile plaques in brain slices from 19-month-old transgenic mice. However, there were no plaques found in the age-matched littermate (SI Fig. 7). These results further confirmed our *in vivo* imaging data that the CRANAD-2 probe could penetrate the BBB and label senile plaques specifically *in vivo*.

Experimental section

General material and methods are available from the supplemental information. Synthetic amyloid-β peptide (1–40) was purchased from rPeptide (Bogart, GA, 30622) and aggregates for *in vitro* studies were generated followed the reported procedure. [37,39] Transgenic Tg2576 mice [38] and littermates were purchased from Taconic Farm, Balb/c mice for BBB penetrating test were obtained from Jackson Laboratory, and the experiment procedure was approved by Massachusetts General Hospital. *In vivo* imaging was recorded on Kodak Imaging Station 2000MM.

Synthesis of CRANAD-1 and CRANAD-2

The synthesis of CRANAD-1 was performed according to the reported procedure [36].

Synthesis of CRANAD-2—2,2-difluoro-1,3-dioxaboryl-pentadione was synthesized using a modified procedure. [29] 1,3-pentadione (0.1g, 1.0 mmol) and trifluoroboron ether (0.2g, 1.0mmol) were mixed together, and the resulting solution was heated at 60 °C for 2 h.. After cooling to the room temperature, the reaction mixture was subjected to evaporation under vacuum, and yellow pale semisolid was obtained, which was solidified with longer standing at room temperature to give a yellow pale needle crystal. The above crystals (0.15g, 0.1mmol) were dissolved in acetonitrile (3.0 ml), followed by the additions of triethylamine (0.30g, 3.0mmol) and 4-*N*,*N*'-dimethyl-benzaldehyde (0.30g, 2.0mmol). The resultant was stirred at 60°C overnight. A black residue was obtained after removing the solvent, and was subjected to flash column chromatography with methylene chloride to give a black powder (63.0mg, yield: 15.0%). ^{1}H NMR (DMSO-*d6*) δ(ppm) 3.04 (s, 12H), 6.26 (s, 1H), 6.79 (m, 6H), 7.68 (d, 4H, J = 8.0 Hz), 7.82 (d, 2H, J = 16Hz); ^{13}C NMR (DMSO-*d6*) δ(ppm) 40.3, 101.0, 111.5, 112.5, 115.1, 122.2, 132.2, 146.5, 153.3, 177.3; ^{19}F NMR (DMSO-*d6*) δ(ppm) −138.9; M/Z: 433 (M+Na).

***In vitro* Aβ aggregates binding constant measurement—**To PBS solutions (1.0 mL) of Aβ40 aggregates (5.0 μM, calculation based on Aβ40 peptide concentration), various amounts of CRANAD-2 were added to the final concentration of 2.5, 5.0, 10.0, 20.0, 40.0, 60.0, 100.0 150.0, 200.0, 250.0, 300.0 nM, and their fluorescence intensities at 715nm were recorded (Ex: 640 nm). The Kd binding curve was generated by software Prism 3.0 with nonlinear one-site binding regression. By measuring the fluorescence intensity of CRANAD-2 alone in PBS buffer (50.0, 100.0, 350.0, 850.0, 1200.0 nM), we confirmed that there was no self-quenching of the dye within the range of the above tested concentrations.

In vivo* NIR imaging—In vivo* NIR imaging was performed using Kodak Imaging station 2000MM. For fluorescence excitation, three laser diodes at 660 nm with a total power of 10 mW/cm2 have been used yielding a uniform illumination of the whole animal. The fluorescent light emitted from the sample (mouse) was detected by a charge-coupled device (CCD) camera (Hamamatsu ORCA) equipped with a focusing lens system (macro lens 60 mm, 1:2.8, Nikon). The image matrix comprised of 532×256 pixels. A bandpass filter was used for the selection of the detection wavelength (700 nm). Integration time default was selected at 30 s. Images were acquired using Kodak 1DTM 3.6.3 Network software and analysed using the KodakTM 1D Analysis software.

Mice (n = 3 for Tg2576 and n = 3 for the littermates) were shaved before background imaging, and were i.v. injected CRANAD-2 (5.0 mg/kg, 20% DMSO, 80% propylene glycol). Fluorescence signals from the brain were recorded at pre-injection, 30, 60, 120, and 240 min. after intravenous injection of the probe. To evaluate our imaging results, an ROI was drawn around the brain region. The data were analyzed by normalizing fluorescence intensity to background fluorescence of each mouse (i.e $F_{(t)}/F_{(pre)}$), where $F_{(t)}$ is the fluorescence intensity of the time point interested, $F_{(pre)}$ is the background fluorescence signal. P values were calculated by Student test.

Ex vivo histological correlation—19 month-old mice and corresponding littermates were injected CRANAD-2 (5.0 mg/kg), scarified at 120 min after injection and perfused with 4% formaldehyde. The brain were excised and embedded in OCT. For microscopy, the brain were sliced into 25 micron slices, each slice was equilibrated for 5 min, and covered with VectaShield mounting media.

Conclusion

In this study we report on the design, synthesis and testing of a novel NIR Aβ plaque-specific fluorescent probe, CRANAD-2. This probe is the first example of difluoroborate diketone compounds for *in vivo* biological studies, which provides a new type of NIR fluorescent dye for cell, tissue, and *in vivo* imaging for small animals. The new probe meets the requirements of a NIR probe for detecting Aβ deposits non-invasively *in vivo*. Currently, investigation of the feasibility of the probe for longitude monitoring of low molecular weight Aβ species (such as oligomers, prefibrilar and fibrils) *in vivo* is underway. Because CRANAD-2 enters brain and binds to amyloid plaques specifically, a radiolabeled version would be suitable for PET imaging. In addition, because of the promise of curcumin as a treatment for AD, we believe that CRANAD-2 might have potential as a therapeutic for this and other diseases.

Supplementary Material

Refer to Web version on PubMed Central for supplementary material.

Acknowledgments

This work was partially supported by the NIH program project grant AG026240 (BJ Bacskai).

REFERENCES

1. Selkoe DJ. Nature 1999;399:A23–A31. [PubMed: 10392577]
2. Stokin GB, Lillo C, Falzone TL, Brusch RG, Rockenstein E, Mount SL, Raman R, Davies P, Masliah E, Williams DS, Goldstein LS. Science 2005;307:1282–1288. [PubMed: 15731448]
3. Meyer-Luehmann M, Spires-Jones TL, Prada C, Garcia-Alloza M, de Calignon A, Rozkalne A, Koenigsknecht-Talboo J, Holtzman DM, Bacskai BJ, Hyman BT. Nature 2008;451:720–724. [PubMed: 18256671]
4. Dubois B, et al. Lancet Neurol 2007;6:734–746. [PubMed: 17616482]
5. Klunk W, et al. Ann. Neurol 2004;55:306–319. [PubMed: 14991808]
6. Hintersteiner M, Enz A, Frey P, Jaton AL, Kinzy W, Kneuer R, Neumann U, Rudin M, Staufenbiel M, Stoeckli M, Wiederhold KH, Gremlich HU. Nat. Biotechnol 2005;23:577–583. [PubMed: 15834405]
7. Skovronsky DM, Zhang B, Kung MP, Kung HF, Trojanowski JQ, Lee VM. Proc. Natl. Acad. Sci. U S A 2000;97:7609–7614. [PubMed: 10861023]
8. Nesterov EE, Skoch J, Hyman BT, Klunk WE, Bacskai BJ, Swager TM. Angew. Chem. Int. Ed. Engl 2005;44:5452–5456. [PubMed: 16059955]
9. Higuchi M, Iwata N, Matsuba Y, Sato K, Sasamoto K, Saido TC. Nat. Neurosci 2005;8:527–533. [PubMed: 15768036]
10. Poduslo JF, Curran GL, Peterson JA, McCormick DJ, Fauq AH, Khan MA, Wengenack TM. Biochemistry 2004;43:6064–6075. [PubMed: 15147190]
11. Jack CR Jr, Garwood M, Wengenack TM, Borowski B, Curran GL, Lin J, Adriany G, Grohn OH, Grimm R, Poduslo JF. Magn. Reson. Med 2004;52:1263–1271. [PubMed: 15562496]
12. Lee VM. Proc. Natl. Acad. Sci. U S A 2001;98:8931–8932. [PubMed: 11481462]
13. Wadghiri YZ, Sigurdsson EM, Sadowski M, Elliott JI, Li Y, Scholtzova H, Tang CY, Aguinaldo G, Pappolla M, Duff K, Wisniewski T, Turnbull DH. Magn. Reson. Med 2003;50:293–302. [PubMed: 12876705]
14. Garcia-Alloza M, Borrelli LA, Rozkalne A, Hyman BT, Bacskai BJ. J. Neurochem 2007;102:1095–1104. [PubMed: 17472706]
15. Bacskai BJ, Frosch MP, Freeman SH, Raymond SB, Augustinack JC, Johnson KA, Irizarry MC, Klunk WE, Mathis CA, Dekosky ST, Greenberg SM, Hyman BT, Growdon JH. Arch. Neurol 2007;64:431–434. [PubMed: 17353389]
16. D'Amore JD, Kajdasz ST, McLellan ME, Bacskai BJ, Stern EA, Hyman BT. J. Neuropathol. Exp. Neurol 2003;62:137–145. [PubMed: 12578223]
17. Weissleder R, Pittet M. Nature 2008;452:580–589. [PubMed: 18385732]
18. Li Q, Lee JS, Ha C, Park CB, Yang G, Gan WB, Chang YT. Angew. Chem. Int. Ed. Engl 2004;43:6331–6335. [PubMed: 15558663]
19. Raymond SB, Skoch J, Hills ID, Nesterov EE, Swager TM, Bacskai BJ. Eur. J. Nucl. Med. Mol. Imaging 2008;35:S93–S98. [PubMed: 18236039]
20. Shishodia S, Sethi G, Aggarwal BB. Ann. N. Y. Acad. Sci 2005;1056:206–217. [PubMed: 16387689]
21. Siwak DR, Shishodia S, Aggarwal BB, Kurzrock R. Cancer 2005;104:879–890. [PubMed: 16007726]
22. Aggarwal BB, Shishodia S, Takada Y, Banerjee S, Newman RA, Bueso-Ramos CE, Price JE. Clin. Cancer Res 2005;11:7490–7498. [PubMed: 16243823]
23. Aggarwal S, Ichikawa H, Takada Y, Sandur SK, Shishodia S, Aggarwal BB. Mol. Pharmacol 2006;69:195–206. [PubMed: 16219905]
24. Yang F, Lim GP, Begum AN, Ubeda OJ, Simmons MR, Ambegaokar SS, Chen PP, Kayed R, Glabe CG, Frautschy SA, Cole GM. J. Biol. Chem 2005;280:5892–5901. [PubMed: 15590663]
25. Ryu EK, Choe YS, Lee KH, Choi Y, Kim BT. J. Med. Chem 2006;49:6111–6119. [PubMed: 17004725]

26. Roth HJ, Miller B. Arch. Pharm. (Weinheim) 1964;297:617–623. [PubMed: 14341926]
27. Roth HJ, Miller B. Arch. Pharm. Ber. Dtsch. Pharm. Ges 1964;297:660–673. [PubMed: 5212809]
28. Zhang G, Chen J, Payne SJ, Kooi SE, Demas JN, Fraser CL. J. Am. Chem. Soc 2007;129:8942–8943. [PubMed: 17608480]
29. Hales JM, Zheng S, Barlow S, Marder SR, Perry JW. J. Am. Chem. Soc 2006;128:11362–11363. [PubMed: 16939253]
30. Chow YL, Johansson CI. J. Phys. Chem 1995;99:17558–17565.
31. Cogné-Laage E, Allemand J-F, Ruel O, Baudin J-B, Croquette V, Blanchard-Desce M, Jullien L. Chem. Eur. J 2004;10:1445–1455.
32. Pfister A, Zhang G, Zareno J, Horwitz AF, Fraser CL. ACS Nano 2008;2:1252–1258. [PubMed: 19081748]
33. Ulrich G, Ziessel R, Harriman A. Angew. Chem. Int. Ed. Engl 2008;47:1184–1201. [PubMed: 18092309]
34. Crews, P.; Rodriguez, J.; Jaspars, M., editors. Organic Structure Analysis. Oxford University Press; 1998.
35. Zhao H, Neamati N, Hong H, Mazumder A, Wang S, Sunder S, Milne GW, Pommier Y, Burke TR Jr. J. Med. Chem 1997;40:242–249. [PubMed: 9003523]
36. Weber WM, Hunsaker LA, Abcouwer SF, Deck LM, Vander Jagt DL. Bioorg. Med. Chem 2005;13:3811–3820. [PubMed: 15863007]
37. Klunk WE, Wang Y, Huang GF, Debnath ML, Holt DP, Mathis CA. Life Sci 2001;69:1471–1484. [PubMed: 11554609]
38. Hsiao K, Chapman P, Nilsen S, Eckman C, Harigaya Y, Younkin S, Yang F, Cole G. Science 1996;274:99–102. [PubMed: 8810256]
39. Jun S, Saxena S. Angew. Chem. Int. Ed. Engl 2007;46:3959–3961. [PubMed: 17427167]

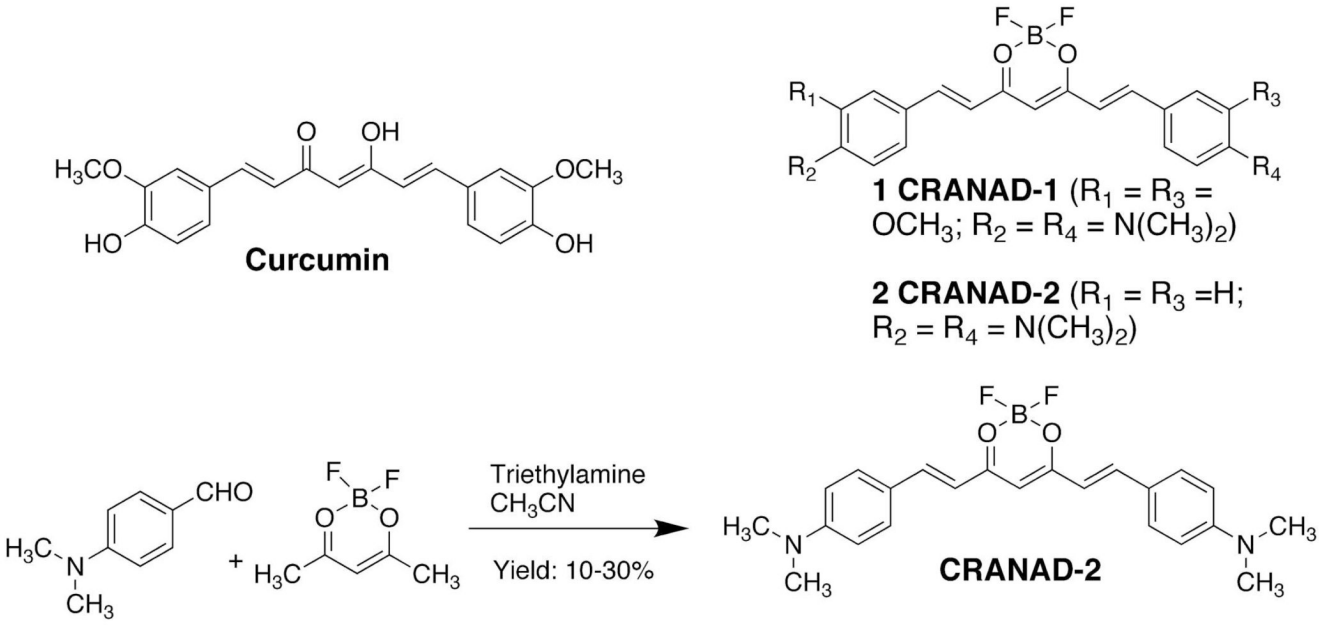

Fig. 1.

The structure of curcumin, compound **1** (CRANAD-1), and compound **2** (CRANAD-2) (top), and the synthetic route for CRANAD-2 (bottom); NMR spectra for CRANAD-2 is shown in SI Fig.2.

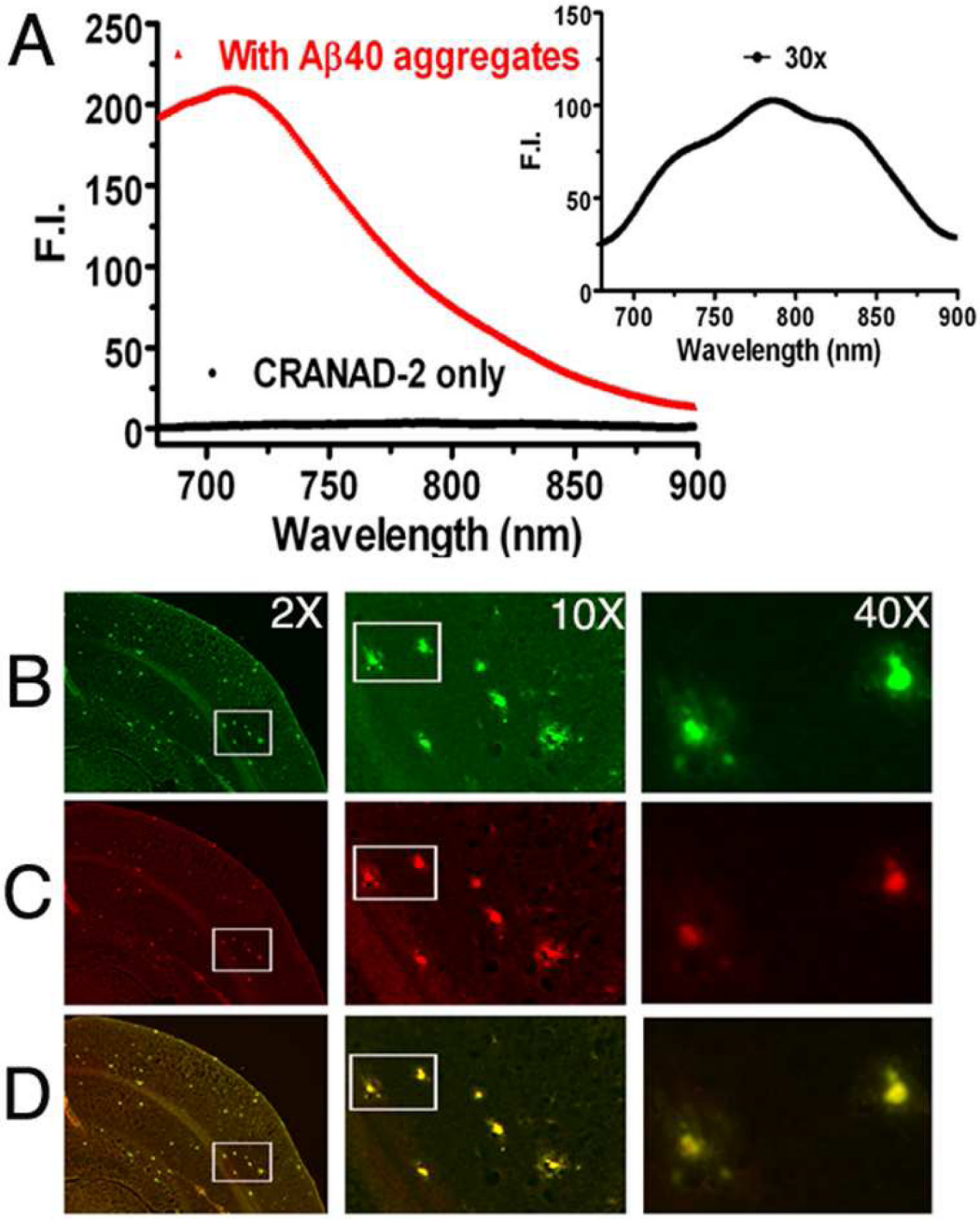

Fig. 2.

A: Fluorescence "turn-on" of CRANAD-2 (100 nM) induced by Aβ aggregates (red line); CRANAD-2 alone in PBS (black line); inset: CRANAD-2 only (Emission intensity is amplified 30 fold). (B–D): Histological staining of the brain slices from an APP-PS1 transgenic mouse. (B) Staining with Thioflavin T indicated abundant plaques in the cortex region; Magnification: left − 2X, middle − 10X, the region highlighted in the left panel, right − 40X, the region highlighted in the middle panel; (C) Staining with CRANAD-2; (D) Merged images of B and C.

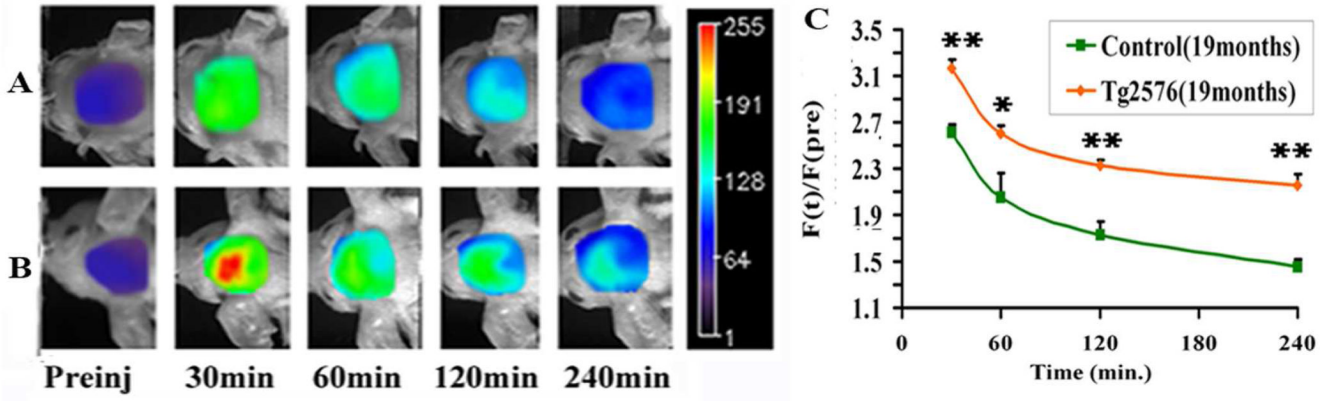

Fig. 3.

Representative images of Tg2576 mice and control littermates at different time points before and after i.v. injection of 5.0 mg/kg of CRANAD-2. (A) 19-month old control mouse; (B) 19-month old Tg2576 mouse (mice showed similar background fluorescence signal). (C) The relative fluorescence signal ($F_{(t)}/(F_{(pre)}$) was significant higher than that of the control mice, and the decay of fluorescence signal was significantly slower in transgenic mice compared to the control group (*: p = < 0.05, **: p = < 0.01);